Growth rate of Rayleigh-Taylor turbulent mixing layers with the foliation approach

Olivier Poujade[*] and Mathieu Peybernes
CEA, DAM, DIF, F-91297 Arpajon, France
(Received 15 July 2009; published 26 January 2010)

For years, astrophysicists, plasma fusion, and fluid physicists have puzzled over Rayleigh-Taylor turbulent mixing layers. In particular, strong discrepancies in the growth rates have been observed between experiments and numerical simulations. Although two phenomenological mechanisms (mode-coupling and mode-competition) have brought some insight on these differences, convincing theoretical arguments are missing to explain the observed values. In this paper, we provide an analytical expression of the growth rate compatible with both mechanisms and is valid for a self-similar, low Atwood Rayleigh-Taylor turbulent mixing subjected to a constant or time-varying acceleration. The key step in this work is the presentation of *foliated* averages and foliated turbulent spectra highlighted in our three-dimensional numerical simulations. We show that the exact value of the Rayleigh-Taylor growth rate not only depends upon the acceleration history but is also bound to the power-law exponent of the foliated spectra at large scales.

I. INTRODUCTION

If allowed to evolve long enough, the Reynolds number of a Rayleigh-Taylor (RT) flow [1,2] increases and the mixing eventually becomes fully turbulent [3,4]. Then, at late time, the width of the mixing layer grows according to

$$L(t) = \alpha_p \mathcal{A} g(t) t^2, \qquad (1)$$

when the gravitational field history [5] is of the form $g(t) \propto t^p$. The Atwood number $\mathcal{A}$ quantifies the density contrast of the initially pure fluids and is tied to the acceleration in any buoyant flow. From a purely theoretical point of view, the RT growth rate coefficient α_p should be universal if the late stage of the evolution of the mixing zone is self-similar and should only depend upon the exponent p of the gravitational field history. However, even today, the value of "alpha" (α), which is the name given by the "alpha-group collaboration" [3] to $\alpha_p/2$ when $p=0$ (constant acceleration), is still a subject of controversy.

For years, the discrepancy between its value inferred from numerical simulations [3,4,6,7] (initialized with small wavelengths), scattered around 0.05, and its experimental values [8–11], twice as large, has thrown doubt on its universality. Not long ago, the heuristic mode-competition mechanism [12,13] put an end to this paradox: adding a small amount of modes of large wavelength to the perturbation of the initial interface helps increase the value of α and reconciles numerical simulations with laboratory experiments. But, it is also instrumental in demonstrating that the initial conditions in any laboratory experiments do feature these modes of large wavelength triggered by external causes like vibrations and residual motions. Flows of interest (geophysics, atmospheric, and astrophysics [14,15]), to a large extent, are not confined to a laboratory. Orders of magnitude may separate the length scales of the interface perturbation with the geometric size of the flow. This is why, the mode-coupling mechanism, initiated with small wavelength modes, is thought to be realized in astrophysical mixing [4] and other natural flows.

Here, in order to find the theoretical value of the growth rate (α_p), we have adopted a point of view which has been used in the study of homogeneous turbulence (HT) for almost half a century but never investigated in RT turbulent mixing. The "large-scale structure of homogeneous turbulence" [16,17] has been studied to understand the conjectured persistence of big eddies and the decay rate of various physical quantities in turbulent flows. At large scales, the turbulent kinetic energy density spectrum behaves as $E(k) \propto k^s$ where the value of s depends on the initialization of freely decaying HT in a way which is still unclear [18–22]. Bulk quantities of such flows, like turbulent kinetic energy, vary as power laws at late time and their exponents appear solely related to the value of s [23]. That underlines the fact that large-scale spectra have a strong influence on the behavior of the overall flow. The theoretical study of freely decaying HT is made difficult by the fact that large scales are driven by non linear effect (triadic interaction). In contrast, the RT turbulence, although anisotropic, displays a significant difference with freely decaying HT. When plunged in a gravitational field, density fluctuations produce motion through buoyancy. This production mechanism affects all scales [24], even the largest, and produces turbulent kinetic energy at all times. It may not be the dominant effect in the inertial range, as argued in [25,26], but it overcomes non linear transfer mechanism at large scales making the theoretical study of RT turbulence much easier.

Here, we demonstrate that it is possible to display an exact formula for α_p which depends upon p, the exponent of the acceleration history, and s, the power-law exponent at large scales of *foliated* spectra that rise up naturally, along with foliated average, from the theoretical developments hereafter. This foliation procedure is presented in turbulent mixing theory because, among other interesting features, it allows to cancel out the formal effect of pressure in the equations, while keeping its physical effect on the whole mixing zone, making theoretical calculations amenable.

---

*Corresponding author; olivier.poujade@cea.fr

II. TRANSVERSE AVERAGE

A RT mixing occurs whenever two fluids of different density, initially separated by a sharp interface, are subjected to a gravitational field directed from the heavier (density ρ_h) to the lighter (density ρ_l) and when the initial interface is slightly distorted by a perturbation whose spectrum contains modes with sufficiently large wavelengths to overcome viscous effects at the onset. Such a flow, with two incompressible fluids in the low Atwood limit $\mathcal{A} = (\rho_h - \rho_l)/(\rho_h + \rho_l) \ll 1$ (Boussinesq approximation), is governed [27] by a concentration Eq. (2), the Navier-Stokes equation supplemented with a buoyant source term (3), and the incompressibility constraint (4)

$$\partial_t c + (\boldsymbol{u}\boldsymbol{\nabla})c = \kappa\Delta c, \tag{2}$$

$$\partial_t \boldsymbol{u} + (\boldsymbol{u}\boldsymbol{\nabla})\boldsymbol{u} = -\boldsymbol{\nabla}P + 2\mathcal{A}\boldsymbol{g}c + \nu\Delta\boldsymbol{u}, \tag{3}$$

$$\boldsymbol{\nabla}\cdot\boldsymbol{u} = 0, \tag{4}$$

where $c(\boldsymbol{x},t)$ is the mass fraction of the heavy fluid ($c=0$ in pure light fluid and $c=1$ in pure heavy fluid), $\boldsymbol{u}(\boldsymbol{x},t)$ the velocity field, and $p(\boldsymbol{x},t)$ the pressure field. The molecular diffusivity κ and the kinematic viscosity of the mixture ν are both assumed to be constant. The gravitational acceleration vector $\boldsymbol{g}(t)$ points down and its intensity may be time dependent as outlined earlier. In our simulations (described in the Sec. VII), the flow fills a rectangular box of size $H \times H \times 2H$ (see Fig. 1 for more details).

The calculation starts by averaging Eqs. (2)–(4). The transverse spatial average of a physical quantity q at height z is defined according to

$$\bar{q}(z,t) = \frac{1}{H^2}\int_{H^2} dxdy\, q(x,y,z,t), \tag{5}$$

along with its fluctuating part $q'(x,y,z,t) = q(x,y,z,t) - \bar{q}(z,t)$. Velocity, concentration, and pressure fields can be decomposed into mean and fluctuating parts: $\boldsymbol{u} = \bar{\boldsymbol{u}} + \boldsymbol{u}'$, $c = \bar{c} + c'$, and $p = \bar{p} + p'$. The velocity along the z axis will be called u_z and $\boldsymbol{v}$ will denote the transverse component in the xy plane so that $\boldsymbol{u} = (\boldsymbol{v}, u_z)$. The divergence Eq. (4) and the fact that vertical velocity cancels at the top and bottom walls yield $\overline{u_z}(z,t) = 0$. Similarly, in a transverse plane at height z, there is an equal probability of finding v_i and $-v_i$ (right/left symmetry in the experimental setup); thus, $\overline{v_i} = 0$, $\overline{v_i'c'} = 0$, and $\overline{v_i'u_z'} = 0$ at all times [27] ($i = x,y$). The behavior of the fluctuating flow will be studied at large scales (low k) and at high Reynolds number. Viscous and diffusive terms (in factor of ν and κ) can then be discarded because in the spectral domain, they contribute a factor νk^2 and κk^2. These terms become important only after a time $t \sim 1/(\nu k^2)$. That happens after a time H^2/ν, or H^2/κ, for viscous, or diffusive, terms at large-scale $k \sim 1/H$. This is well above $\sqrt{H/(\mathcal{A}g)}$ (the time required by the RT mixing zone to grow and to fill the domain of width H) since H is well above $\Delta \sim (\nu^2/\mathcal{A}g)^{1/3}$ (Δ being the mesh size as in [3]). Therefore, the resulting set of equations governing the evolution of the fluctuating flow at large scales reads
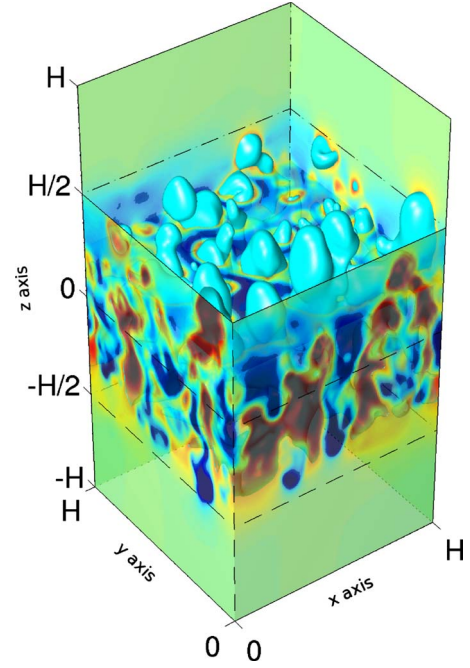

FIG. 1. (Color online) Image of a turbulent Rayleigh-Taylor mixing zone for a constant acceleration ($p=0$) when $L(t)=H$ from our numerical simulations. The axes are defined in such a way that the mixing zone grows along z and is spatially periodic along x and y. The initial interface between pure light fluid and pure heavy fluid is located at $z=0$. Thus, along the z axis at time t, the flow goes from a turbulent mixing of two fluids when $|z| < L(t)/2$ to an intermittent border at $|z| \approx L(t)/2$ and finally to a laminar pure fluid (light or heavy depending upon the direction) when $|z| > L(t)/2$. The vertical velocity u_z' of the flow is plotted in false color on the vertical sections. It puts to the fore large structures going up (light gray/red) and down (dark/blue), made up of mixed fluids. The 3D bubblelike shapes on top (at $z \approx H/2$) correspond to isosurfaces of u_z' at 80% of its maximum positive value.

$$\partial_t c' + u_z'\partial_z\bar{c} + \partial_i(v_i'c') + \partial_z(u_z'c') = \partial_z\overline{u_z'c'}, \tag{6}$$

$$\partial_t u_z' + \partial_j(v_j'u_z') + \partial_z(u_z'u_z') - \partial_z(\overline{u_z'u_z'}) = -\partial_z p' - 2\mathcal{A}gc', \tag{7}$$

$$\partial_t v_i' + \partial_j(v_j'v_i') + \partial_z(u_z'v_i') - \partial_j(\overline{v_j'v_i'}) = -\partial_i p', \tag{8}$$

where Einstein summation convention is used on the repeated indices i and $j \in \{x,y\}$.

III. FOLIATED AVERAGE

The last equations can be Fourier transformed for the purpose of showing that the growth rate of a RT mixing zone depends upon the structure of turbulence at large scales. Since the physical domain is assumed to be periodic along x and y (see Fig. 1), one defines a Fourier transform operator acting on these two directions only (transverse directions). It turns a generic quantity $f(\boldsymbol{r},z,t)$, where $\boldsymbol{r} = (x,y)$ is the transverse position, into $\widetilde{f}(\boldsymbol{k},z,t)$, where $\boldsymbol{k} = (k_x,k_y)$ is the transverse wave vector. Equations (6)–(8) become
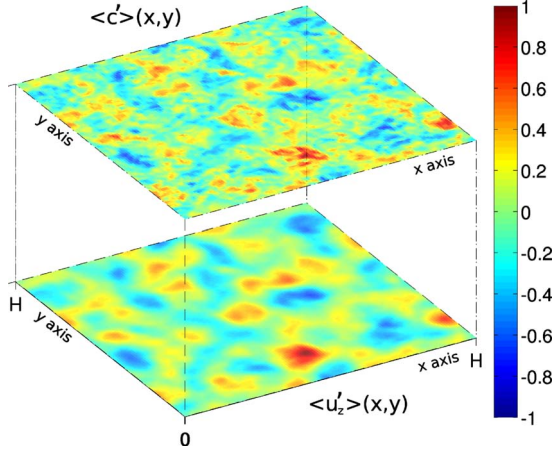
FIG. 2. (Color online) Image of the foliated concentration and of the foliated vertical velocity. The top slice displays $\langle c'\rangle(x,y)$ in false color at the instant when $L(t)=H$ for $p=0$. The bottom slice displays $-\langle u'_z\rangle(x,y)$ (the minus sign is introduced so that colors match between top and bottom). On the color chart, the value 1 corresponds to the normalized maximum. The striking similarity in location and shape of large scales on both planes (peculiar to foliated average) reveals that heavy mixed fluid tends to concentrate where the flow goes down (dark/blue) and light mixed fluid where the flow goes up (light gray/red).

$$\partial_t \widetilde{c'} = -\widetilde{u'_z}\partial_z\bar{c} - \partial_z(\widetilde{u'_z*c'}) - \imath k_j \widetilde{v'_j*c'}, \qquad (9)$$

$$\partial_t \widetilde{u'_z} = -\partial_z(\widetilde{u'_z*u'_z}) - \partial_z\widetilde{p'} - 2\mathcal{A}g\widetilde{c'} - \imath k_j\widetilde{v'_j*u'_z}, \quad (10)$$

$$\partial_t \widetilde{v'_i} = -\partial_z(\widetilde{u'_z*v'_i}) - \imath k_i\widetilde{p'} - \imath k_j\widetilde{v'_j*v'_i}, \qquad (11)$$

where $*$ is the usual folded product. In order to simplify Eqs. (9)–(11), one can eliminate the effect of ∂_z, and with it, the effect of pressure and non locality, by integrating these equations along the anisotropic direction z. Therefore, these arguments suggest introducing the foliated spatial average which, for a physical quantity q, is defined according to

$$\langle q\rangle(x,y,t) = \frac{1}{H}\int q(x,y,z,t)dz. \qquad (12)$$

It amounts to chopping the domain (foliation) in elementary slices, transverse to the anisotropic direction, and to squeezing them by adding them up, resulting in an effective two-dimensional (2D) flow (see Fig. 2). Both in the concentration Eq. (9) and in the equation of motion (10), $\langle \partial_z(\widetilde{u'_z*q'})\rangle=0$ (where $q'=c'$ or u'_z) because at top and bottom walls $\widetilde{u'_z}=0$. The average of the pressure gradient is $\langle \partial_z\widetilde{p'}\rangle=0$ because pressure fluctuations decrease outside the mixing zone. It has to be assumed that the top and bottom walls are far enough so that $\lim_{z\to\pm\infty}\widetilde{p'}(z,\boldsymbol{k},t)=0$. Consequently, the boundaries do not affect the flow within the mixing zone if $L(t)\ll 2H$ (which can be relaxed to $L(t)\lesssim H$ in simulations). This is why, the resulting concentration equation and equation of motion after foliated average are

$$\partial_t\langle\widetilde{c'}\rangle = -\langle\widetilde{u'_z}\partial_z\bar{c}\rangle - \imath k_j\langle\widetilde{v'_j*c'}\rangle, \qquad (13)$$

$$\partial_t\langle\widetilde{u'_z}\rangle = -2\mathcal{A}g\langle\widetilde{c'}\rangle - \imath k_j\langle\widetilde{v'_j*u'_z}\rangle. \qquad (14)$$

In Eq. (13), the term $\langle\widetilde{u'_z}\partial_z\bar{c}\rangle$ can be simplified because, at small Atwood number, the profile of $\bar{c}(z,t)$ deviates only from a straight line (constant slope) at the edges of the mixing zone. This approximation is corroborated experimentally [10,11] and numerically, in our simulations ($\mathcal{A}=0.1$), to within statistical fluctuations due, at a given height z, to the finite number $N(t)\approx H^2/\ell(t)^2$ of eddies in the transverse plane of area H^2 [the integral length scale $\ell(t)$, i.e., the diameter of a typical eddy, varies like $L(t)\propto t^{p+2}$ in the self-similar regime and these statistical fluctuations become negligible in the limit $H\to+\infty$ since their rms amplitude is on the order $1/\sqrt{N(t)}\approx\ell(t)/H$]. In this limit, the derivative $\partial_z\bar{c}$ is uniform and equal to $1/L(t)$ within the mixing zone to a good approximation. Thus, the theoretical development suggests defining L such that $\partial_z\bar{c}=1/L(t)$ which can be brought close to another definition of the width at low Atwood number (see the end of Sec. VII). Therefore, and this is the only approximation made in this development, it is possible to write

$$\langle\widetilde{u'_z}\partial_z\bar{c}\rangle \approx \langle\widetilde{u'_z}\rangle\partial_z\bar{c} = \langle\widetilde{u'_z}\rangle/L(t). \qquad (15)$$

The contribution of the edges is negligible in the foliated average because it represents a small portion of the integration domain. As a consequence, (i) at large scale [$k\ll 2\pi/\ell(t)$], (ii) at low Atwood (iii) at high Reynolds number, and (iv) in the limit $H\to+\infty$ [i.e., $L(t)\ll H$], the evolution of foliated second moments can be derived. From Eqs. (13) and (14), straightforward algebraic manipulations provide

$$\partial_t(\langle\widetilde{c'}\rangle\langle\widetilde{c'}\rangle^*) = -\frac{2\,\mathrm{Re}[\langle\widetilde{u'_z}\rangle\langle\widetilde{c'}\rangle^*]}{L(t)} - k_j\xi^c_j, \qquad (16)$$

$$\partial_t(\langle\widetilde{u'_z}\rangle\langle\widetilde{u'_z}\rangle^*) = -4\mathcal{A}g\,\mathrm{Re}[\langle\widetilde{u'_z}\rangle\langle\widetilde{c'}\rangle^*] - k_j\xi^z_j, \qquad (17)$$

$$\partial_t(\mathrm{Re}[\langle\widetilde{u'_z}\rangle\langle\widetilde{c'}\rangle^*]) = -2\mathcal{A}g\langle\widetilde{c'}\rangle\langle\widetilde{c'}\rangle^* - \frac{\langle\widetilde{u'_z}\rangle\langle\widetilde{u'_z}\rangle^*}{L(t)} - k_j\xi^{cz}_j, \qquad (18)$$

where $\xi^c_j=2\,\mathrm{Re}[\imath\langle\widetilde{v'_j*c'}\rangle\langle\widetilde{c'}\rangle^*]$, $\xi^z_j=2\,\mathrm{Re}[\imath\langle\widetilde{v'_j*u'_z}\rangle\langle\widetilde{u'_z}\rangle^*]$, and $\xi^{cz}_j=\mathrm{Re}[\imath\langle\widetilde{v'_j*u'_z}\rangle\langle\widetilde{c'}\rangle^*]+\mathrm{Im}[\imath\langle\widetilde{v'_j*c'}\rangle\langle\widetilde{u'_z}\rangle^*]$ cancelled out when ensemble averaged.

IV. ENSEMBLE AVERAGED FOLIATED SPECTRA

Let us note $\hat{q}$ the ensemble average of a generic quantity q. Different realizations of the RT flow have the same initial spectrum of interface perturbations but the initial phases of the modes are different and are generated at random. As a result, if one realization is initialized with a set of random phases, called $\Phi(\boldsymbol{k},t=0)$, and produces $\xi_j(\boldsymbol{k},t)$, then the particular realization initialized with phases $\Phi(\boldsymbol{k},t=0)+\pi$ will produce $-\xi_j(\boldsymbol{k},t)$ with the exact same probability. When

averaged, these two contributions cancel out and therefore the ensemble average over all possible realizations—or equivalently, over all possible initializations—translates into $\widehat{\hat{\xi}_j^c}(\boldsymbol{k},t)=0$, $\widehat{\hat{\xi}_j^z}(\boldsymbol{k},t)=0$, and $\widehat{\hat{\xi}_j^{cz}}(\boldsymbol{k},t)=0$.

It suggests defining the ensemble averaged foliated spectra for kinetic energy, concentration and production, respectively, as

$$\mathcal{E}_z(k,t)=\frac{k}{2}\int d\Omega \widehat{\langle \widetilde{u_z'}\rangle \langle \widetilde{u_z'^*}\rangle},\tag{19}$$

$$\mathcal{E}_c(k,t)=k\int d\Omega \widehat{\langle \widetilde{c'}\rangle \langle \widetilde{c'^*}\rangle},\tag{20}$$

$$\mathcal{E}_{cz}(k,t)=-k\int d\Omega\ \mathrm{Re}[\widehat{\langle \widetilde{u_z'}\rangle \langle \widetilde{c'^*}\rangle}],\tag{21}$$

where the integration over the solid angle $d\Omega$ is to be understood as the integration over all directions of $\boldsymbol{k}$ (in the transverse plane). The ξs in Eqs. (16)–(18) disappear when ensemble averaged and the ensemble averaged foliated spectra, referred to as foliated spectra for short, are coupled to each other at large scales according to

$$\dot{\mathcal{E}}_c=2\frac{\mathcal{E}_{cz}}{L(t)},\tag{22}$$

$$\dot{\mathcal{E}}_z=2\mathcal{A}g\mathcal{E}_{cz},\tag{23}$$

$$\dot{\mathcal{E}}_{cz}=2\mathcal{A}g\mathcal{E}_c+2\frac{\mathcal{E}_z}{L(t)}.\tag{24}$$

It should be stressed that this closed set of equations does not hold if foliated average operators are removed or even replaced by transverse average because of the non local effect of pressure. Since these equations are linear, autonomous in k, and do not display derivatives with respect to k, it comes as a byproduct prediction of the theory that, with the aforementioned definitions, all three foliated spectra must have the same power-law exponent at large scales: k^s. The exponent s is independent of time to comply with self-similarity. This common value is a special feature of the foliated spectra (see Fig. 3). Foliated spectra have deliberately been designated by script $\mathcal{E}$ in order to stress the difference with transverse spectra classically defined by

$$E_z(k,z,t)=\frac{k}{2}\int d\Omega \widetilde{u_z'}\widetilde{u_z'^*},\tag{25}$$

$$E_c(k,z,t)=k\int d\Omega \widetilde{c'}\widetilde{c'^*},\tag{26}$$

$$E_{cz}(k,z,t)=-k\int d\Omega\ \mathrm{Re}[\widetilde{u_z'}\widetilde{c'^*}].\tag{27}$$

Both types of spectrum were compared to show that this common exponent is specific to the foliated spectra whereas
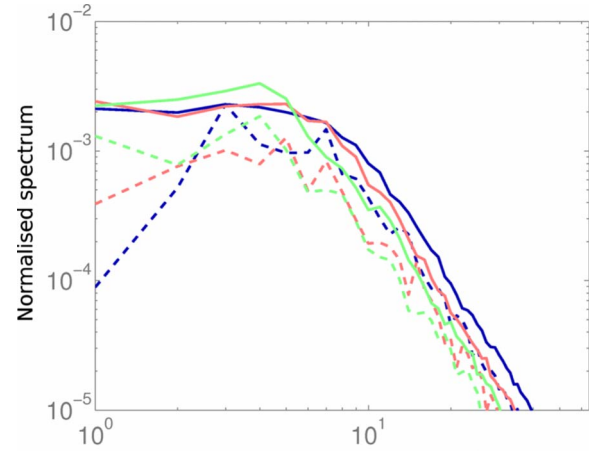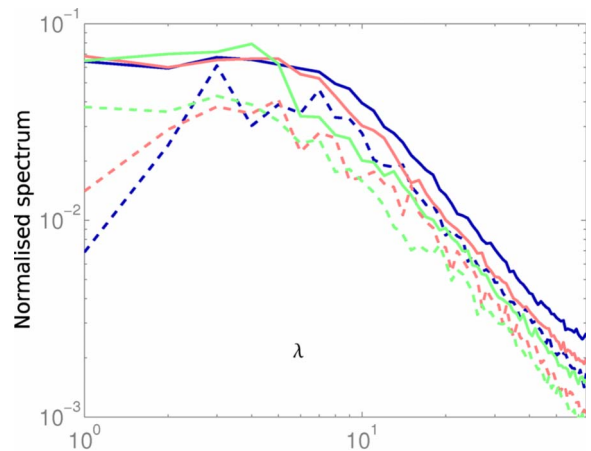
FIG. 3. (Color online) Normalized foliated spectra versus transverse spectra. The left figure represents the ratio of velocity and concentration spectra, $\mathcal{E}_z(k)/[\mathcal{E}_c(k)g(t)L(t)]$ in solid lines and $E_z(k)/[E_c(k)g(t)L(t)]$ in dashed lines. The right figure represents the ratio of production and concentration spectra, $\mathcal{E}_{cz}(k)/(\mathcal{E}_c(k)\sqrt{g(t)L(t)})$ in solid lines and $E_{cz}(k)/(E_c(k)\sqrt{g(t)L(t)})$ in dashed lines. Displayed results come from the simulation at constant acceleration $p=0$. The colors correspond to different times in the evolution of the mixing zone: t_1 (dark/blue), $<t_2$ (medium gray/red), and $<t_3$ (light gray/green) defined by $L(t_1)=0.5H$, $L(t_2)=0.75H$, and $L(t_3)=H$. In the whole domain of wave numbers, ratios of foliated spectra are distinctively smoother than transverse spectra. In the domain where $n<6$ (large scales), the ratio of *foliated* spectra is constant and does not vary with time whereas, in the same domain, the ratio of transverse spectra can vary up to one decade.

transverse spectra (concentration and velocity for instance) have different power-law exponents [7] at large scales. This can be understood when realizing that a transverse spectrum is calculated using Fourier modes on a slice at a height z in the middle of the mixing zone. A foliated spectrum, on the other hand, uses the sum along z of all these modes. The resulting spectrum is radically different and benefits from interferences between modes at different heights.
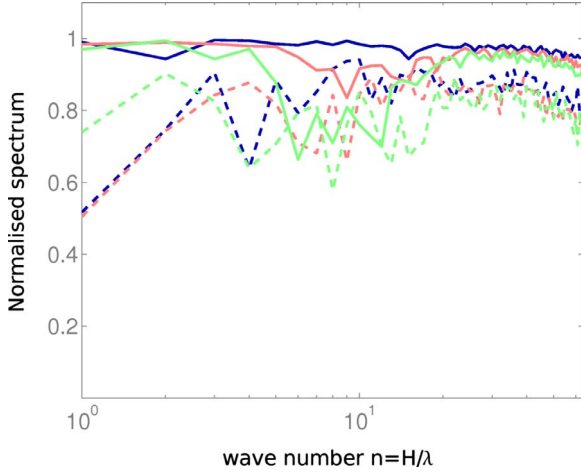
FIG. 4. (Color online) Normalized correlation spectra. The evolution of $\mathcal{R}(k,t)=\mathcal{E}_{cz}^2(k,t)/2\mathcal{E}_z(k,t)\mathcal{E}_c(k,t)$ (solid lines) and of $R(k,t)=E_{cz}^2(k,t)/2E_z(k,t)E_c(k,t)$ (dashed lines) at constant acceleration $p=0$ is compared at different times, t_1 (dark/blue), $<t_2$ (medium gray/red), and $<t_3$ (light gray/green). The simulation, at $p=0$ (but at $p=1$, 2 and 3 as well), shows that when $n\leq6$, $\mathcal{R}=1$ to within 6% and with the same characteristic smoothness as already depicted on Fig. 2 (vertical axis is linear). On the contrary, R varies significantly as time goes by on the same range of wave numbers.

V. GROWTH RATE FORMULA

For self-similarity to hold, the late time behavior of the foliated spectra must be

$$\mathcal{E}_z(k,t) = \mathcal{E}_z^0 k^s t^{e_z}, \tag{28}$$

$$\mathcal{E}_c(k,t) = \mathcal{E}_c^0 k^s t^{e_c}, \tag{29}$$

$$\mathcal{E}_{cz}(k,t) = \mathcal{E}_{cz}^0 k^s t^{e_{cz}}, \tag{30}$$

at low k where $\mathcal{E}_c^0$, $\mathcal{E}_z^0$, and $\mathcal{E}_{cz}^0$ are constants independent from k and t. In addition, the exponent of k in each of this averaged spectrum (s) and the time exponents (e_c, e_z, e_{cz}) must be constant in time. When replacing these expressions with $\mathcal{A}g(t)=\mathcal{A}g_p t^p$ and $L(t)=\alpha_p\mathcal{A}g_p t^{p+2}$ in Eqs. (22)–(24) one gets the following relations:

$$e_z = e_c + 2(p+1), \tag{31}$$

$$e_{cz} = e_c + (p+1), \tag{32}$$

$$\mathcal{E}_z^0 = [\alpha_p(\mathcal{A}g_p)^2 e_c/e_z]\mathcal{E}_c^0, \tag{33}$$

$$\mathcal{E}_{cz}^0 = (\alpha_p\mathcal{A}g_p e_c/2)\mathcal{E}_c^0, \tag{34}$$

$$\alpha_p = \frac{8}{e_z e_c}, \tag{35}$$

which come straight from Eqs. (2)–(4) within the approximation made in Eq. (15). Using Eqs. (28) and Eqs. (31)–(35), a nontrivial exact result can be deduced: $\mathcal{E}_{cz}^2(k,t)/[2\mathcal{E}_z(k,t)\mathcal{E}_c(k,t)]=1$ valid at large scale (see Fig. 4).

A fundamental feature of concentration is that its fluctuation variance, $\overline{c'c'}$ tends to a constant in the self-similar regime because concentration is a physical quantity bounded between 0 and 1. It cannot go to zero for that would mean the mixing tends to be heterogeneous in the middle of the mixing zone, thereby going against the fact that at all times any side of the mixing zone must be supplied with pure fluid from the other side. The mixed-fluid supplying channels have been highlighted in Figs. 1 and 2. This is exemplified by numerical simulations and experiments reporting molecular mixing rates ranging from 0.7 to 0.8 [3,4,10,27].

The question now is: how about $\langle c'\rangle\langle c'\rangle$? A very simple argument can be given: the discretized foliated average,

$$\langle c'\rangle = dz/H \sum_{i=-H/dz}^{H/dz} c_i', \tag{36}$$

can be approximated by

$$\langle c'\rangle = dz/H \sum_{i=-L(t)/dz}^{L(t)/dz} c_i', \tag{37}$$

since c' is only nonzero within the mixing zone. That is why,

$$\langle c'\rangle\langle c'\rangle \approx dz^2/H^2 \sum_{i=-L(t)/dz}^{L(t)/dz} \sum_{j=-L(t)/dz}^{L(t)/dz} c_i' c_j', \tag{38}$$

$$\overline{\langle c'\rangle\langle c'\rangle} \approx dz^2/H^2 \sum_{i=-L(t)/dz}^{L(t)/dz} \sum_{j=-L(t)/dz}^{L(t)/dz} c_0^2 \delta_{ij}, \tag{39}$$

if we say $\overline{c'c'}=c_0^2$ in the self-similar regime as described in the previous paragraph. Therefore,

$$\overline{\langle c'\rangle\langle c'\rangle} \approx dz^2/H^2 \sum_{i=-L(t)/dz}^{L(t)/dz} c_0^2 = dz/H^2 L(t) c_0^2. \tag{40}$$

As a result $\overline{\langle c'\rangle\langle c'\rangle}$ must grow like $L(t)$ (corroborated by our numerical simulations).

Therefore, since $\overline{\langle c'\rangle\langle c'\rangle}=\int_0^{+\infty} dk\mathcal{E}_c(k,t)$ varies as $\int_0^{2\pi/\ell(t)\propto t^{-p-2}} dk\mathcal{E}_c(k,t) \propto t^{e_c-(p+2)(s+1)}$ and must evolve as $L(t) \propto t^{p+2}$, the value of e_c is bound to be $(p+2)(s+2)$ and, by inference, the time exponents $e_z=(p+2)(s+2)+2(p+1)$ and $e_{cz}=(p+2)(s+2)+(p+1)$. Therefore, the value of the Rayleigh-Taylor growth rate for the turbulent mixing zone width, α_p, is shown to depend upon p, which is the acceleration exponent, and s, the foliated spectrum power-law exponent at large scales, according to

$$\alpha_p(s) = \frac{8}{(p+2)(s+2)[p(s+4)+2(s+3)]}. \tag{41}$$

This expression does not depend on g_p as expected and confirmed in our simulations.

The demonstration leading to this formula did not provide any arguments against the idea of an s varying with p. However, growth rates, at various values of p given by our simulations in conjunction with those provided in [28], were fitted to the theoretical formula and a remarkable collapse of the data was found for $s=4.0\pm0.1$ assuming s was independent of p (see Fig. 5). It is possible to check this result by using an
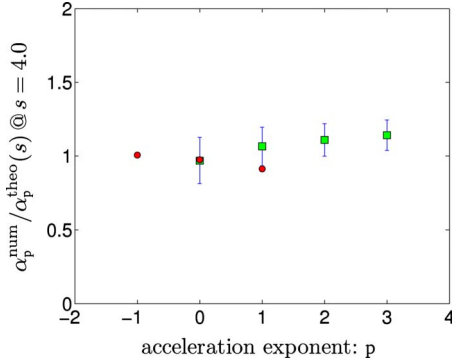
FIG. 5. (Color online) Observed to predicted ratio of growth rate α_p. Green squares correspond to results obtained with SURFER and performed by the authors and red circles to results performed with TURMOIL3D by D. Youngs and A. Llor. A least square best fit has been applied on the numerical results using the formula (41) and it was found, assuming s does not depend on p, that $s = 4.0 \pm 0.1$. Error bars correspond to the size of the biggest interval containing all three different measures of α_p: (1) $\alpha_p = L(t)/(\mathcal{A}g(t)t^2)$, (2) $\alpha_p = \dot{L}(t)/[(p+2)\mathcal{A}g(t)t]$, and (3) the same method described in Ref. [4]. Error bars were not provided in Ref. [28].

other obvious method: direct inspection of the foliated *spectra*. The power law at large scales of foliated spectra was checked on every simulation ($p = 0$, 1, 2, and 3) and was found to be compatible with $s = 4$. The formula (41) is therefore a predictive formula: it gives the value of α_p knowing p (a controlled parameter) and s or, the other way around, it gives s knowing p and α_p. Our theory did not provide a value for s for it certainly depends upon the way the mixing flow reaches the self-similar regime. Moreover, RT turbulence in 2D is totally different from RT in three-dimensional (3D) [25,29]. This dependence of α_p upon spatial dimension is hidden in the value of s. In order to find its value, the theory would have to cope with the transition regime to make the connection with the linear growth of the initial conditions ($s = 4$ seems to be compatible with annular spectrum initial conditions in 3D). It must be emphasized that the result (41) is a proof that, in the self-similar regime, the growth of the mixing zone only depends upon the structure of turbulence at large scales (apart from p, it depends on s only).

VI. IMPLICATIONS

Obviously, the formula for α_p carries information on the dynamics of the mixing zone width. Not so obvious is the fact that it also provides information on the way this dynamic affects the mixing at large scale. If it is assumed that the late time evolution of the mixing zone width does not depend upon initial conditions—which may be true when the characteristic length scale of the initial perturbations is much smaller than that of the physical domain H—it is reasonable to admit that it must depend on $L(t)$ (and its derivatives) and $g(t)$ which are the only control parameters left in the problem. From this assumption, basis of the buoyancy-drag approach [8,30], it is possible to build a simple evolution equation,

$$\ddot{L}(t) = C_b \mathcal{A}g(t)L(t) - C_d \dot{L}^2(t)/L(t), \qquad (42)$$

which depends on two adjustable constants. The constant C_b quantifies buoyancy related to the mixing since $C_b \mathcal{A}$ can be seen as an effective Atwood number: the fluids are not pure, with density ρ_l and ρ_h, in the mixing zone but they are partly mixed with intermediate densities and the smaller C_b, the smaller the effective Atwood number and the stronger the mixing. The constant C_d quantifies drag, i.e., the exchange of momentum between raising and falling mixed-fluids structures. This phenomenological approach does not by itself provide any relation between these two adjustable constants. However, replacing the self-similar values (1) of L and g in Eq. (42) allows to recover the exact formula (41) if and only if $C_b = 4/(s+2)$ and $C_d = (s+2)/2$, which yields $C_b = 2/C_d$. This correspondence between the simple model and the exact result demonstrate the little importance of small scale as opposed to large scale in the bulk dynamics of the mixing. Furthermore, it enables to understand the influence of s on "intuitive" physical mechanisms like buoyancy, through the effective Atwood number, and drag. Accordingly, the bigger s, the stronger the drag, the smaller the effective Atwood number and the better the mixing.

This is in agreement with numerical results [12,13] suggesting that a smaller proportion of long wavelength in the spectrum (bigger s: mode-coupling) decreases the growth rate of the mixing zone width in opposition to a bigger proportion of long wavelength (smaller s: mode-competition). Therefore, in the framework of foliated spectra where s is defined, the two phenomenological mechanisms of mode-coupling and mode-competition in Rayleigh-Taylor turbulent mixing can be explained and brought together.

There is no reason in principle why techniques developed in this work could not be applied to other mixing flows with one anisotropic direction. For instance, in the case of Richtmyer-Meshkov (RM) turbulence [30], $\mathcal{A}g = 0$ and the mixing width $L(t)$ varies like t^θ in Eqs. (22)–(24). Persistence of big eddies [16] is then an exact result for the foliated RM flow since the right-hand side of Eq. (23) vanishes. The same type of reasoning that led to Eq. (41) allows to find $\theta = 2/(s+4)$ (also an exact result when s is the power-law exponent of ensemble averaged foliated spectra at large scale) which for $3 \leq s \leq 4$ predicts a $1/4 = 0.250 \leq \theta \leq 0.286 = 2/7$, in agreement with experimental and numerical results.

VII. SIMULATIONS

A set of four simulations of Rayleigh-Taylor turbulent mixing flows were carried out with the incompressible code SURFER [31] for different acceleration histories $g(t) \propto t^p$ with $p = 0$, $p = 1$, $p = 2$, and $p = 3$. For our purpose, gravity was added to the original version.

An incompressible code is valuable to investigate flows under variable acceleration because hydrostatic pressure balances instantaneously with the acceleration field. On the contrary, a compressible simulation would have to cope with the creation of acoustic waves that would travel at the speed of sound to balance pressure with time-varying acceleration. These acoustic waves would bounce on the domain walls,

would go back and forth through the simulation domain and would be detrimental to the simulations.

Each of those simulations was performed with the same grid resolution: $128 \times 128 \times 256$ (along x, y, and z, respectively). The large scale outcomes of a numerical simulation of a Rayleigh-Taylor turbulent flow do not vary significantly, for a given type of initial condition, by increasing the resolution. This explains the choice of such a modest resolution allowing to carry out more simulations.

SURFER is parallelized, 3D and evolves two immiscible fluids separated by an interface. To reconstruct and advance the fluid interfaces in time, SURFER uses an exactly volume conserving variant of the Volume of Fluid algorithm with a Piecewise Linear Interface Calculation method (VOF/PLIC) [32]. The density of each fluid ρ_h (for heavy) and ρ_l (for light fluid) are constant in time. The Navier-Stokes equation governing the evolution of the velocity field $\boldsymbol{u}$ is given by

$$\rho \frac{d\boldsymbol{u}}{dt} = -\boldsymbol{\nabla} p + \boldsymbol{\nabla} \cdot (\eta \boldsymbol{S}) + \sigma r \delta_S \boldsymbol{n} + \rho \boldsymbol{g}, \qquad (43)$$

where ρ is the density, p is the pressure and $\boldsymbol{g}$ is the acceleration. The dynamic viscosity η equals $\eta_h = \rho_h \nu$ or $\eta_l = \rho_l \nu$ (where ν is a common kinematic viscosity) and $\boldsymbol{S}$ is the rate of strain tensor defined by $S_{ij} = \partial_i u_j + \partial_j u_i$. The surface tension σ depends on the particular two fluids that will be heterogeneously mixed and the delta function, δ_S, is concentrated on the surface of the interface, r is the mean curvature of this surface and $\boldsymbol{n}$ is the unit normal on the surface. The discretization of Eq. (43) is performed on a marker-and-cell-type staggered grid and the pressure is computed using an iterative multigrid Poisson solver.

The simulations were carried out in nondimensional units. Initially, two vertically stacked fluid layers of different density, such that $\mathcal{A} = 0.1$, have been considered (see Fig. 1). Periodic boundary conditions were prescribed on the four vertical domain walls, whereas no flux and no slip conditions were imposed on the two horizontal walls of the domain, at the top and at the bottom. Initially, the velocity field $\boldsymbol{u}(x,y,z,t=0)$ is perturbed around the interface using a sum of random small amplitude modes which comply with the incompressibility condition. The wave numbers selected verify $15 \le n \le 17$ ($n \gg 1$) to get a late time self-similar evolution of the flow (mode-coupling mechanism). Kinematic viscosity ν and surface tension σ in Eq. (43) were chosen in such a way that they affect small scales only (large $k \approx 2\pi/\Delta$ where Δ is the mesh size). This is why $\mathcal{A}g/\Delta \approx \nu^2/\Delta^4$ and $\mathcal{A}g/\Delta \approx \sigma/(\rho\Delta^3)$. Therefore, $\nu \approx \sqrt{\mathcal{A}g\Delta^3}$, as in [3], and $\sigma \approx \rho \mathcal{A}g\Delta^4$. It is important to stress that the interface reconstruction mimics the effect of a small molecular diffusion coefficient $\kappa \ll \nu$.

The value of α_p is affected by how the width of the mixing zone, $L(t)$, is measured or computed. Experimentally and numerically, two methods are employed and they both use $\bar{c}(z,t)$. The threshold method prescribes $L_{\text{th}}(t) = |z_{99} - z_1|$ where $\bar{c}(z_1,t) = 0.01$ and $\bar{c}(z_{99},t) = 0.99$. This method is affected by statistical fluctuations of $\bar{c}$ producing noisy $L_{\text{th}}(t)$ and an even noisier derivative. The integral method prescribes $L_{\text{int}}(t) = 6\int dz\, \bar{c}(z,t)[1 - \bar{c}(z,t)]$ which provides an exact value if the profile of $\bar{c}$ is linear. Since $\bar{c}$ is almost affine everywhere in our simulation at low Atwood, the difference between $L_{\text{int}}(t)$ and $1/\partial_z \bar{c}$ is negligibly small. In a sense, the reasoning that led to the growth rate formula dictated the definition of L, by the integral method, which has been used to calculate the value of α_p in each of the four simulations.

[1] L. Rayleigh, Proc. Lond. Math. Soc. **14**, 170 (1883).
[2] G. I. Taylor, Proc. R. Soc. London, Ser. A **201**, 192 (1950).
[3] G. Dimonte *et al.*, Phys. Fluids **16**, 1668 (2004).
[4] W. Cabot and A. Cook, Nat. Phys. **2**, 562 (2006).
[5] A. Llor, Laser Part. Beams **21**, 305 (2003).
[6] A. W. Cook, W. Cabot, and P. L. Miller, J. Fluid Mech. **511**, 333 (2004).
[7] W. Cabot, Phys. Fluids **18**, 045101 (2006).
[8] G. Dimonte and M. Schneider, Phys. Fluids **12**, 304 (2000).
[9] G. Dimonte and M. Schneider, Phys. Rev. E **54**, 3740 (1996).
[10] N. Wilson and M. J. Andrews, Phys. Fluids **14**, 938 (2002).
[11] A. Banerjee and M. J. Andrews, Phys. Fluids **18**, 035107 (2006).
[12] G. Dimonte, P. Ramaprabhu, D. L. Youngs, M. J. Andrews, and R. Rosner, Phys. Plasmas **12**, 056301 (2005).
[13] P. Ramaprabhu, G. Dimonte, and M. J. Andrews, J. Fluid Mech. **536**, 285 (2005).
[14] A. J. Aspden, J. B. Bell, M. S. Day, S. E. Woosley, and M. Zingale, Astrophys. J. **689**, 1173 (2008).
[15] M. R. Krumholz, Science **323**, 754 (2009).
[16] G. K. Batchelor and I. Proudman, Phil. Trans. R. Soc. A **248**, 369 (1956).
[17] P. G. Saffman, J. Fluid Mech. **27**, 581 (1967).
[18] P. A. Davidson, J. Turbul. **1**, 6 (2000).
[19] T. Ishida, P. A. Davidson, and Y. Kaneda, J. Fluid Mech. **564**, 455 (2006).
[20] P. A. Davidson, *Turbulence. An Introduction for Scientists and Engineers* (Oxford University Press, New York, 2004).
[21] M. Lesieur and S. Ossia, J. Turbul. **1**, 7 (2000).
[22] S. Ossia and M. Lesieur, J. Turbul. **1**, 10 (2000).
[23] J. R. Chasnov, Phys. Fluids **7**, 600 (1995).
[24] O. Poujade, Phys. Rev. Lett. **97**, 185002 (2006).
[25] M. Chertkov, Phys. Rev. Lett. **91**, 115001 (2003).
[26] G. Boffetta, A. Mazzino, S. Musacchio, and L. Vozella, Phys. Rev. E **79**, 065301(R) (2009).
[27] J. R. Ristorcelli and T. T. Clark, J. Fluid Mech. **507**, 213 (2004).
[28] D. Youngs and A. Llor, *Proceedings of the International Work-*

shop on the Physics of Compressible Turbulent Mixing, Pasadena (2001).

[29] A. Celani, A. Mazzino, and L. Vozella, Phys. Rev. Lett. **96**, 134504 (2006).

[30] G. Dimonte, Phys. Plasmas **7**, 2255 (2000).

[31] B. Lafaurie, C. Nadone, R. Scardovelli, S. Zaleski, and G. Zanetti, J. Comput. Phys. **113**, 134 (1994) SURFER can be downloaded at http://www.lmm.jussieu.fr/zaleski/codes/.

[32] D. Gueyffier *et al.*, J. Comput. Phys. **152**, 423 (1999).